

# Effect of strain rate and fibre rotation on the in-plane shear response of $\pm 45^\circ$ laminates in tension and compression tests

Hao Cui<sup>a1</sup>, Daniel Thomson<sup>a</sup>, Antonio Pellegrino<sup>a</sup>, Jens Wiegand<sup>b</sup>, Nik Petrinic<sup>a</sup>

<sup>a</sup>Department of Engineering Science, University of Oxford. Oxford, UK

<sup>b</sup>COMPACT Composite Impact Engineering LTD, Manchester, UK

## Abstract

This work focuses on the effect of strain rate and fibre rotation on the in-plane shear properties of composite laminates. The effect of fibre rotation on the measured shear properties, was for the first time experimentally quantified with the comparison between compression and tension tests of the  $\pm 45^\circ$  laminate samples. Significant increase of shear strength and decrease of final failure strain was observed with the increase in strain rate from  $5 \times 10^{-4}$  1/s to 1300 1/s. The nonlinear constitutive model was developed to simulate the large deformation process, in which the fibre orientation was updated as a function of the in-plane shear strain. The results of this investigation should motivate the updating of procedures for experimental characterization as well as analytical and numerical modelling of in-plane shear response of laminates.

**Key words:** in-plane shear; fibre rotation; rate-dependent; Hopkinson bar;  $\pm 45^\circ$  laminate

## 1. Introduction

Carbon fibre composite laminates feature high stiffness and strength in fibre orientation, while their elastic moduli as well as strength in transverse direction are relatively weak. Inter-fibre failure is one of the dominating failure modes for composite laminates, and significant nonlinearities may occur prior to fracture in composite structures. Considerable nonlinearity of in-plane behaviour has been observed in off-

---

<sup>1</sup> Correspond author: [hao.cui@eng.ox.ac.uk](mailto:hao.cui@eng.ox.ac.uk), +44 (0)1865613452, Parks Road, Oxford, OX1 3PJ

axis compression tests of unidirectional laminates, and it has been found to be dependent on the strain rate [1, 2]. The shear properties of laminated composites are very important for predicting permanent deformation and damage, and several models have been developed [3-6]. In this study, the rate dependent in-plane shear properties were characterized using  $\pm 45^\circ$  laminates, in order to gain deeper understanding of their nonlinear deformation behaviour, and to support the development of constitutive models for simulation of composites subjected to impact loading.

The in-plane shear response can be obtained from off-axis compression/tension tests. Achieving large deformations poses several challenges, as the deformation process becomes unstable once damage has initiated [1, 2]. The  $\pm 45^\circ$  laminates yield quite uniform shear stress distribution over the whole gauge area [7], and provide stable damage evolution for large deformation. However, the tension test of  $\pm 45^\circ$  exhibit significant fibre rotation [8]. The reinforcement fibres get more aligned with the loading axis as the shear strain increases during tests, resulting in the overestimation of the shear stress, as confirmed with analytical and numerical work [9, 10]. The opposite trend may be observed when the compression loading is applied, and this can be used in comparison with tension tests to evaluate the influence of fibre rotation on measured shear response.

This paper aims to study the rate-dependence in in-plane shear, and to reveal the effect of fibre rotation on the laminate response in both experiments and modelling. The experimental setups and related data processing methods are introduced in Section 2. The corresponding numerical models of the specimens and the developed constitutive model used to simulate the conducted experiments are outlined in Section 3. All results and discussions are presented in Section 4, followed by concluding remarks in Section 5.

## 2. Experimentation

### 2.1 Material and Specimen

A 2mm-thick laminate ( $[0/90]_{8s}$ ) was made of HexPly<sup>®</sup> IM7/8552 carbon-epoxy prepreg, a material extensively used in both industry and academic research. The laminate has been inspected using ultra-sound scan to ensure that no large defects or voids were present. The specimens for tension and compression tests were all manufactured by cutting this laminate at the  $45^\circ$  with a water-cooled diamond saw. The gauge section of the dog-bone tension samples was shaped and surface finished using a surface-grinding machine. The geometry of these samples is shown in Fig.1. The tension samples were bonded using 3M Scotch-Weld DP490 adhesive into impedance matched, metallic, threaded end-sleeves for gripping into the loading rigs.

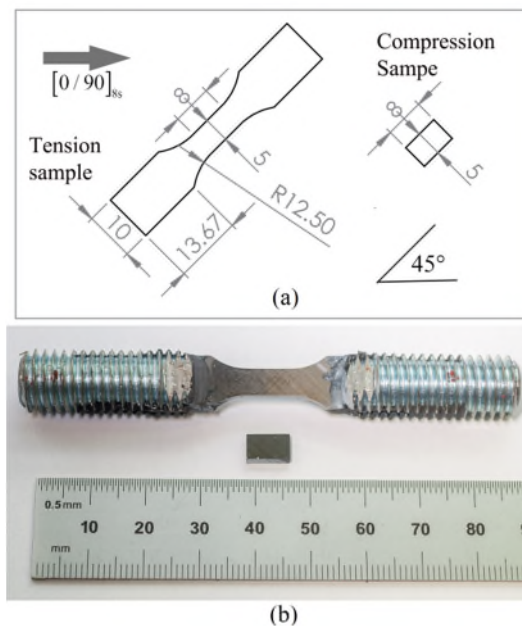


Fig.1 (a) Tension dog-bone sample; (b) compression sample

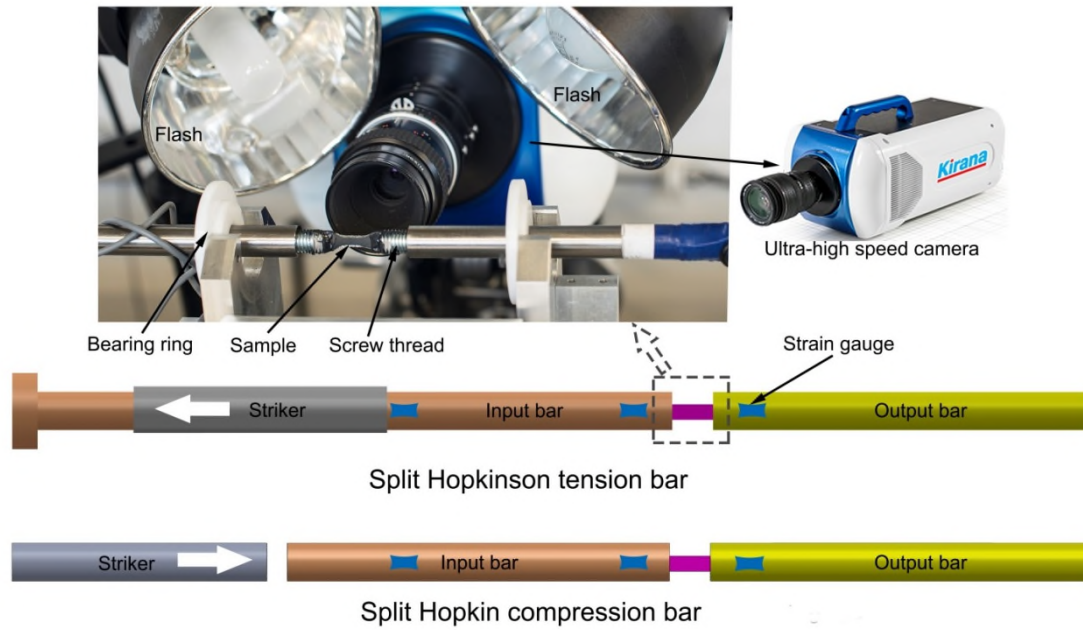


Fig.2 Hopkinson bar systems for dynamic tests

## 2.2 Test setup

The Zwick/Roell Z250 screw driven testing machine with 20KN loading cell was used in quasi-static tests. The displacement controlled loading rate was 0.01mm/s. An in-house built Split-Hopkinson-Tension and Compression Bar systems [11] were used for dynamic tests(Fig.2). The striker velocity was approximately 5m/s in compression tests, and 11m/s in tension tests. Strain gauges were used to acquire the strain history on the split Hopkinson bars, from which the force histories applied upon all samples were calculated. These dynamic experiments are considered valid for the purpose of classical characterisation of mechanical performance on condition that the dynamic equilibrium and strain homogeneity along the sample gauge section are both established during the tests [12, 13]. A 0.5mm-thick cardboard was used to shape the loading pulse in the dynamic compression test thus filtering out undesirable high frequency response of the loading system to the impact loading imposed by the its striker. The relatively long tension samples required a considerably longer time than the compression samples to reach dynamic equilibrium conditions. For that reason, a 3mm-thick rubber sheet was used as pulse shaper to more gradually ramp up the force applied on samples.

The samples were coated with a black speckle pattern on a white background, which enabled displacement and strain measurement across the whole sample surface using digital image correlation (DIC) methodology (in-house [14] and commercial software GOM Aramis were used). Quasi-static tests were recorded with a camera at frame rate of 2 FPS. The ultra-high speed camera SI-Kirana was used in dynamic tests.

### 2.3 Data processing

The displacement (extension and contraction) across the specimens gauge section and the corresponding strain can be evaluated from the images taken during tests by means of the DIC method. The strain distribution within gauge area is reasonably uniform over the gauge section. The average normal strains in both  $x$  and  $y$  directions were calculated from the changing of edge length of the gauge area as:

$$\begin{aligned}\varepsilon_{xx} &= \Delta l_x / l_x \\ \varepsilon_{yy} &= \Delta l_y / l_y\end{aligned}\tag{1}$$

where  $\Delta l_x$  and  $\Delta l_y$  are the elongations, while  $l_x$  and  $l_y$  are the length and width of the gauge area in the direction of parallel and perpendicular to the loading direction. The shear strain is then calculated as:

$$\gamma_{12} = \varepsilon_{xx} - \varepsilon_{yy}\tag{2}$$

The shear stress was calculated considering the change in cross-section:

$$\tau_{12} = \frac{F}{2A}(1 + \varepsilon_{xx})\tag{3}$$

### 2.4 Correction for fibre rotation

The calculation of the shear stress with Eq (3) is accurate for small strain conditions, while the fibre rotation gets pronounced when the strains get large. There is an analytical solution for linear-elastic materials to estimate the ratio between the shear stress  $\tau_{xy}$  at small strains calculated with Eq (3) and the true shear stress  $\bar{\tau}_{xy}$  [10]:

$$f = \frac{\tau_{12}}{\bar{\tau}_{12}} = \frac{(1-\beta)^2(Q_{11}Q_{22} - Q_{12}^2) + 4\beta Q_{66}(Q_{11} + Q_{22} + 2Q_{12})}{4mn(1+\beta)Q_{66}[\beta Q_{11} + Q_{22} + (1+\beta)Q_{12}]} \quad (4)$$

where

$$m = \cos \theta, n = \sin \theta, \beta = n^2/m^2 \quad (5a, 5b, 5c)$$

and  $\theta$  is the fibre orientation. The fibre orientation changes with shear strain, and is calculated here as:

$$\theta = \pi/4 + \lambda \gamma_{12}/2 \quad (6)$$

where  $\lambda$  is equal to  $-1$  for compression tests and  $1$  for tension tests.

The stiffness constants  $Q_{ij}$  are calculated from material properties of unidirectional laminates:

$$\begin{aligned} Q_{11} &= E_{11}/(1 - \nu_{12}\nu_{21}) \\ Q_{12} &= Q_{21} = E_{11}\nu_{21}/(1 - \nu_{12}\nu_{21}) \\ Q_{22} &= E_{22}/(1 - \nu_{12}\nu_{21}) \end{aligned} \quad (7)$$

The material constants in Eq (5) are listed in Table.1.

During large in-plane shear deformation, the moduli in transverse direction,  $E_{22}$ , also get degraded. However, the degraded transverse properties were not possible to be evaluated accurately, and were not considered in this study.

Considering each point of the nonlinear portion of the true shear stress-strain curve as fictitiously “linear elastic”, the reduced shear modulus  $Q_{66}$  decreases with shear strain and is calculated as follows:

$$Q_{66,i} = \tau_{12,i}/\gamma_{12,i} \quad (8)$$

at each data point  $i$  of the small-strain based shear stress-strain response. The corrected shear stress comprising fibre rotation is then calculated as follows:

$$\bar{\tau}_{12} = \tau_{12}/f(Q_{66}, \theta) \quad (9)$$

### 3. Numerical modelling

#### 3.1 Laminate model

The tension and compression experiments were simulated numerically using the finite element method as illustrated in Fig.3. The experimentally acquired boundary conditions were used as input data for modelling. The laminates were modelled with three dimensional 8 node reduced integration solid ‘brick’ element (C3D8R) in Abaqus 6.14, material properties are listed in Table.1.

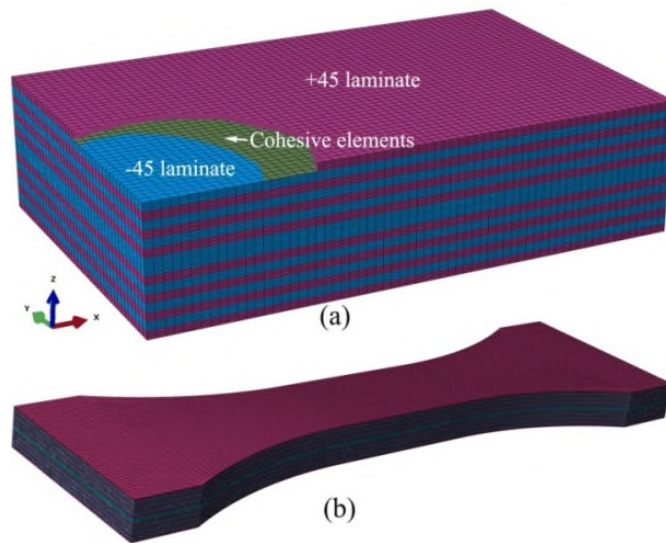


Fig.3 Numerical models for (a) compression tests and (b) tension tests

Due to large in-plane shear, the inter-laminar shear stress  $\tau_{xz}$  and  $\tau_{yz}$  may also exceed its yielding limit in  $\pm 45^\circ$  laminates, whereby this transverse shear deformation concentrates at the resin-rich interface between two layers. To avoid large distortion of bulk elements, the cohesive zone model was used to simulate the nonlinear deformation in X-Z and Y-Z directions. The implemented (as user-defined in Abaqus/Explicit) cohesive law features very high initial stiffness (1e5MPa/mm) before exceeding its reversible limit, to avoid non-physical contribution to the out-of-plane deformation. The inter-laminar cohesive stress after yielding is determined using experimentally determined in-plane shear behaviour.

All simulations were done using Abaqus/Explicit. The quasi-static simulation was carried out using the true density for a long time to avoid any inertia effect generated during rapid fracture processes.

Table.1 Elastic properties of IM7/8552 laminate[15]

$E_{11}$	162095 MPa
$E_{22}$	9721 MPa
$E_{33}$	9721 MPa
$G_{12}$	4688 MPa
$G_{13}$	4688 MPa
$G_{23}$	5000 MPa
$\nu_{12}$	0.362
$\nu_{13}$	0.362
$\nu_{23}$	0.3

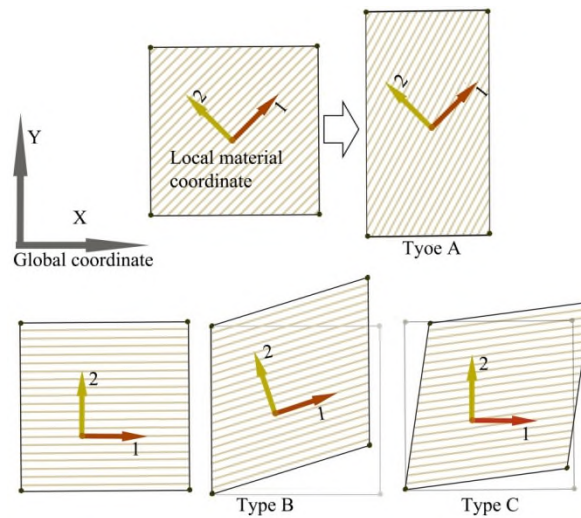


Fig.4 Fibre rotation during shear deformation of unidirectional laminate: the patterns indicate fibre orientation, and the 1-2 axis is the local material coordinate system used FEM

### 3.2 Constitutive model

The local material coordinates should be updated during analysis in order to account for the rotation of fibres due to shear deformation. A single element benchmark study was carried out to verify this functionality in commercial software package Abaqus



6.14. As sketched in Fig.4, the local material orientation was not updated for the shear deformation modes A and C, although these modes dominate in off-axis loaded laminates, with one of them prevailing depending on the alignment of the element topology with respect to the fibre orientation. As a result, in this study, the fibre rotation due to shear deformation was taken into account within the constitutive model, in order to simulate accurately the conducted experiments. A user defined material model was developed to account for the change of fibre rotation due to shear deformation. A user subroutine VUMAT was written, allowing for the continuous calculation of the fibre orientation during simulation. The fibre orientation is calculated as follows:

$$\theta = \arctan \frac{1 - \varepsilon_{xx}}{1 - \varepsilon_{yy}} \quad (10)$$

where  $\varepsilon_{xx}$  is the strain along loading axis and  $\varepsilon_{yy}$  is the strain normal to the loading axis this equation provided very close estimation of fibre rotation in comparison to the Eq(6) used in processing experimental results.

Within the VUMAT, the strain tensor in global coordinates  $\boldsymbol{\varepsilon}_g$  was updated first. The following equation was used to compute the strain in local material coordinates

$$\boldsymbol{\varepsilon} = \mathbf{R}(\theta) \cdot \boldsymbol{\varepsilon}_g \quad (11)$$

where  $\boldsymbol{\varepsilon} = [\varepsilon_{11}, \varepsilon_{22}, \varepsilon_{33}, \varepsilon_{12}, \varepsilon_{23}, \varepsilon_{13}]^T$  is the strain tensor in local material system, and  $\boldsymbol{\varepsilon}_g$  is the strain in global system. The rotation matrix  $\mathbf{R}(\theta)$  is

$$\mathbf{R}(\theta) = \begin{bmatrix} c_2 & s_2 & 0 & 2s_1c_1 & 0 & 0 \\ s_2 & c_2 & 0 & -2s_1c_1 & 0 & 0 \\ 0 & 0 & 1 & 0 & 0 & 0 \\ -s_1c_1 & s_1c_1 & 0 & c_2 - s_2 & 0 & 0 \\ 0 & 0 & 0 & 0 & c_1 & s_1 \\ 0 & 0 & 0 & 0 & -s_1 & c_1 \end{bmatrix} \quad (12)$$

where  $c_2 = c_1^2$ ,  $s_2 = s_1^2$ ,  $s_1 = \sin(\theta)$ ,  $c_1 = \cos(\theta)$ . The normal stress in the local material system is then updated as follows

$$\sigma_{ij} = C_{ij} \varepsilon_{ij} \quad (i=1,2,3; j=1,2,3) \quad (13)$$

where the  $C_{ij}$  is the stiffness tensor calculated as follows

$$\begin{aligned} \chi &= E_{11}E_{22} - E_{11}E_{33}v_{23}^2 - 2E_{22}E_{33}v_{13}v_{23} - E_{22}E_{33}v_{13}^2 \\ C_{11} &= (E_{22} - E_{33}v_{23}^2)E_{11}/\chi \\ C_{12} &= C_{21} = (E_{22}v_{12} + E_{33}v_{13}v_{23})E_{11}E_{22}/\chi \\ C_{13} &= C_{31} = (v_{12}v_{23} + v_{13})E_{11}E_{22}E_{33}/\chi \\ C_{22} &= (E_{11} - E_{33}v_{13}^2)E_{22}^2/\chi \\ C_{23} &= C_{32} = (E_{11}v_{23} + E_{22}v_{12}v_{13})E_{22}E_{33}/\chi \\ C_{33} &= (E_{11} - E_{22}v_{12}^2)E_{22}E_{33}/\chi \end{aligned} \quad (14)$$

The shear stresses  $\tau_{23}$  and  $\tau_{13}$  were updated as follows

$$\begin{aligned} \tau_{23} &= G_{23}\gamma_{23} \\ \tau_{13} &= G_{13}\gamma_{13} \end{aligned} \quad (15)$$

The in plane shear stress  $\tau_{12}$  was controlled by the master curves obtained from tension/compression tests at different loading rates. These master curves were read into the VUMAT at the beginning of computation, and the exact shear stress was determined by interpolation between two neighbouring data points of the curve.

After update of the stress state in the local coordinates system, the stress in the global coordinates can then be calculated as follows

$$\sigma = R(-\theta) \cdot \sigma \quad (15)$$

## 4. Results and Discussions

### 4.1 Force-displacement

The edge surface of the specimens was monitored in quasi-static tests, and the representative damage evolution processes were depicted in Fig.5 at each stage of the load-displacement curves. In tension tests, there is no visible damage occurred at the

moment of yielding. The load dropped slightly after yielding, and micro cracks started to emerge at displacement of 0.6mm. The load carried by the specimen then kept growing causing an increasing number of micro cracks in each ply to appear. There were no delamination cracks observed until the extension of about 1.5mm was reached, which was followed by catastrophic failure. In compression test, the stiffness appears higher because of the shorter length of the sample. There were not many visible cracks on the edge of compression samples, until the contraction of 0.9mm was reached when delamination between layers appeared.

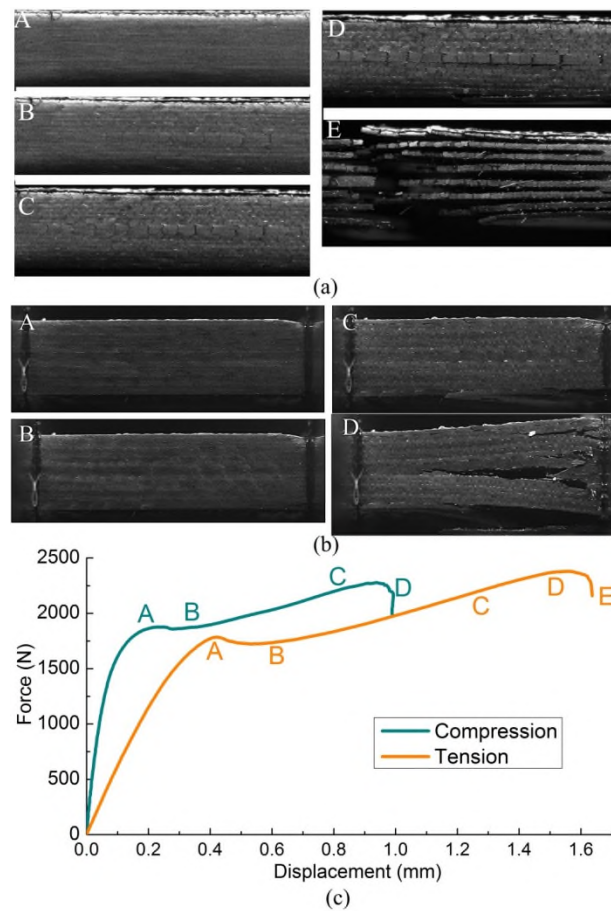


Fig.5 (a) Failure process in quasi-static tension tests; (b) failure process in quasi-static compression; (c) load-displacement curves

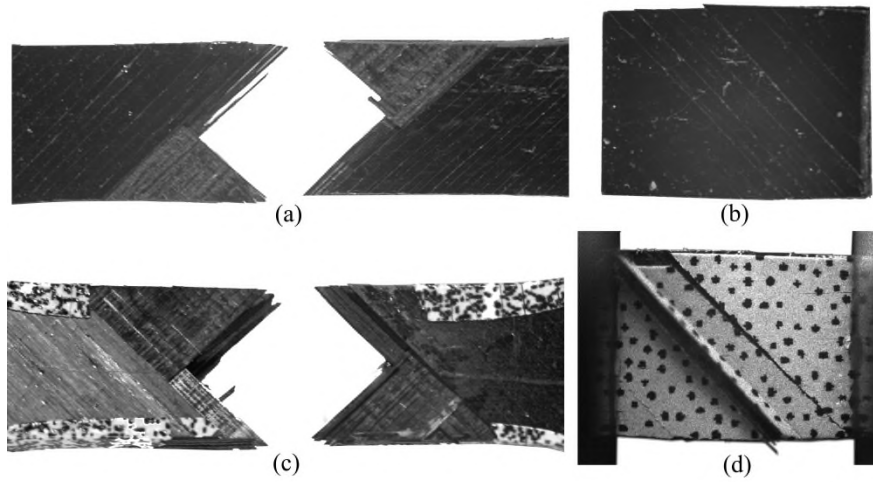


Fig.6 Samples after tests (a) quasi-static tension; (b) quasi-static compression; (c) dynamic tension; (d) dynamic compression

Samples after tension and compression tests in different loading rates are all presented in Fig.6. The delamination between plies of different angles has resulted in the complete break of tension, and the dynamic tests produced similar macroscopic failure pattern as that in quasi-static tests. Detailed investigation on the failure mechanisms in tension tests will be presented in Section 4.5. The cross-section of compression samples in quasi-static tests was analysed and illustrated in Fig.7. Although the delamination seemed to trigger the final failure of the  $\pm 45^\circ$  laminates in both tension and compression load, the number of in-plane crack in compression tests was considerably smaller than in tension. This could be due to the fact that the high hydro-static stress in compression experiments might have prevented the opening of cracks and growth of voids within the epoxy matrix.

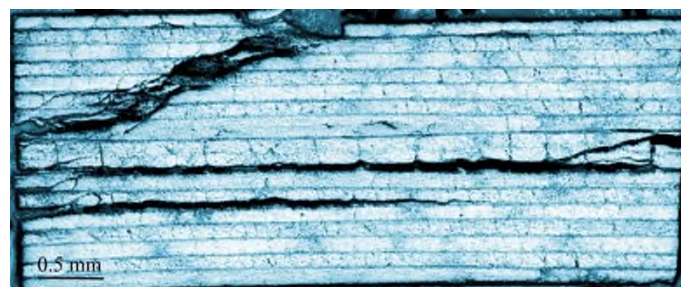


Fig.7 Failure of compression samples in quasi-static tests.

In the dynamic tests, the force at both ends of the sample, calculated from the signal on the input bar and output bar [13], are plotted in Fig.8. The force on one end of the specimen is very similar to that on the other, showing that dynamic equilibrium conditions were achieved from the early stage during experiments. After an initial ramp-up period where the strain rate rapidly increases, a constant strain rate plateau is reached long before failure. Hence, the sample and test setup produced valid measurement of the nonlinear deformation response.

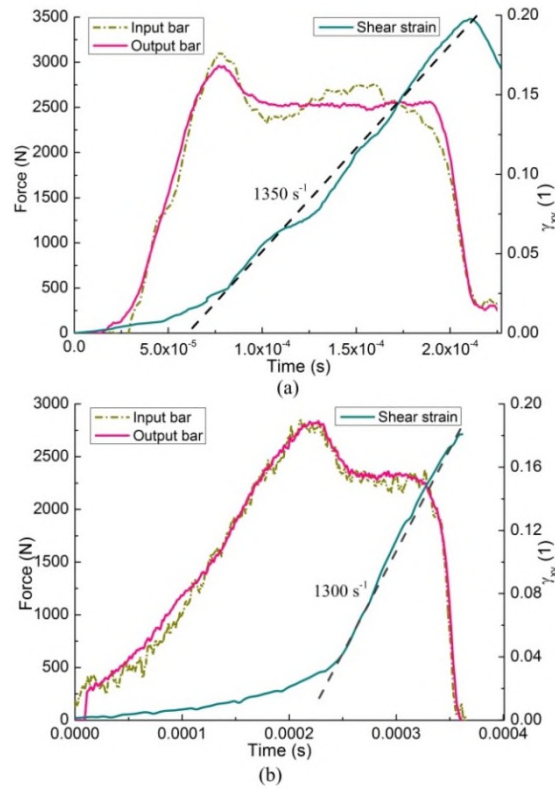


Fig.8 The equilibrium and shear strain in (a) dynamic compression and (b) dynamic tension tests

## 4.2 In-plane shear response

The original shear stress, calculated directly with Eq (3) is plotted in Fig.9 as a function of shear strain. In the quasi-static tests, the shear stress increased with rising tangential shear stiffness after yielding, similar to tests reported in literature [8, 9, 16, 17]. Both tension and compression tests produce quite similar shear response at small strain stage, although the shear stress from compression tests appears slightly higher

than that in tension. The shear stress obtained from dynamic tests exhibits a certain degree of softening process after the elastic phase and then the stress plateaued in compression tests and increased slightly in tension tests. It is interesting to identify that the results from tension and compression start to deviate from each other after shear strain larger than 10% (see the arrow in Fig.9). Considering the fact that the fibres rotate in opposite directions between compression and tension tests, this study indicate that the shear stress are reasonably accurate for strain smaller than 10%.

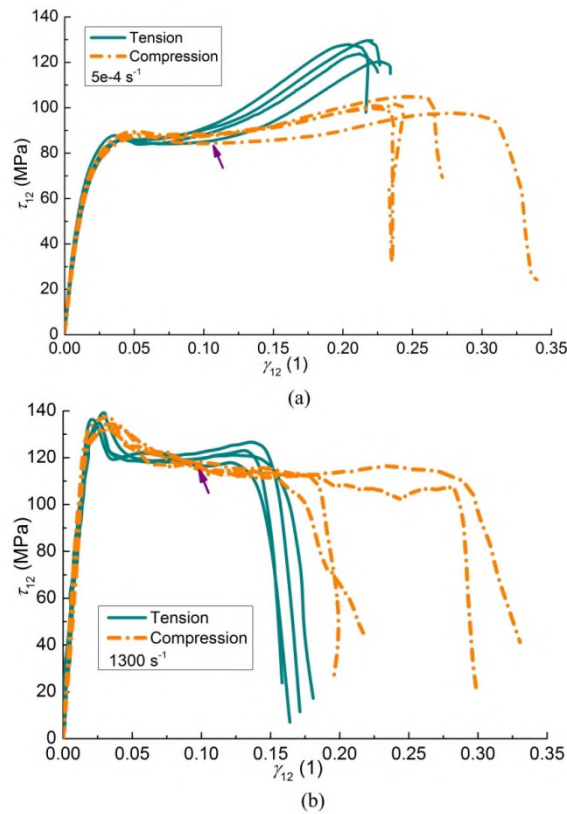


Fig.9 The original stress from tension and compression tests in (a) quasi-static and (b) dynamic rate

### 4.3 Shear response with correction of fibre rotation effect

The analytical solution for estimating the effect of fibre rotation was used in this study to approximate the true in-plane shear behaviour from the original data. The shear stresses look considerably different from the apparent ones after the correction. In particular there was no significant strain hardening beyond the yield, as shown in

Fig.10. The shear strength increased significantly with the strain rate, with similar trends observable in both tension and compression tests. The final failure strain in dynamic tests is smaller than that in quasi-static ones. The shear stress obtained from compression tests is slightly higher than that from tension tests. This may indicate the dependence of in-plane shear response upon hydrostatic pressure [18, 19] and thus caused different deformation and failure mechanisms, as discussed in Section 4.1.

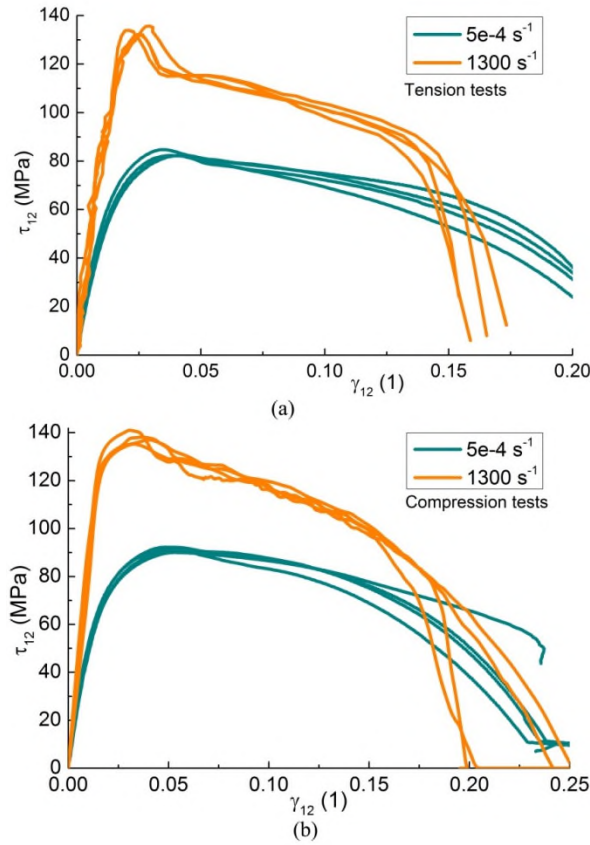


Fig.10 corrected shear from (a) tension tests and (b) compression tests

#### 4.4 Evaluation of experimental results with FEM

In-plane shear model at different strain rate for each test configuration was generated by averaging the experimental results. All tests were simulated with both the small-strain based and corrected shear properties within updating of fibre orientation during computation. The fibre orientation does change with in-plane shear deformation and can be determined kinematically regardless of the material constitutive behaviour. For the purpose of representing existing modelling methods, the small-strain based



shear stress calculation model was also employed to simulate all these tests without updating fibre orientation.

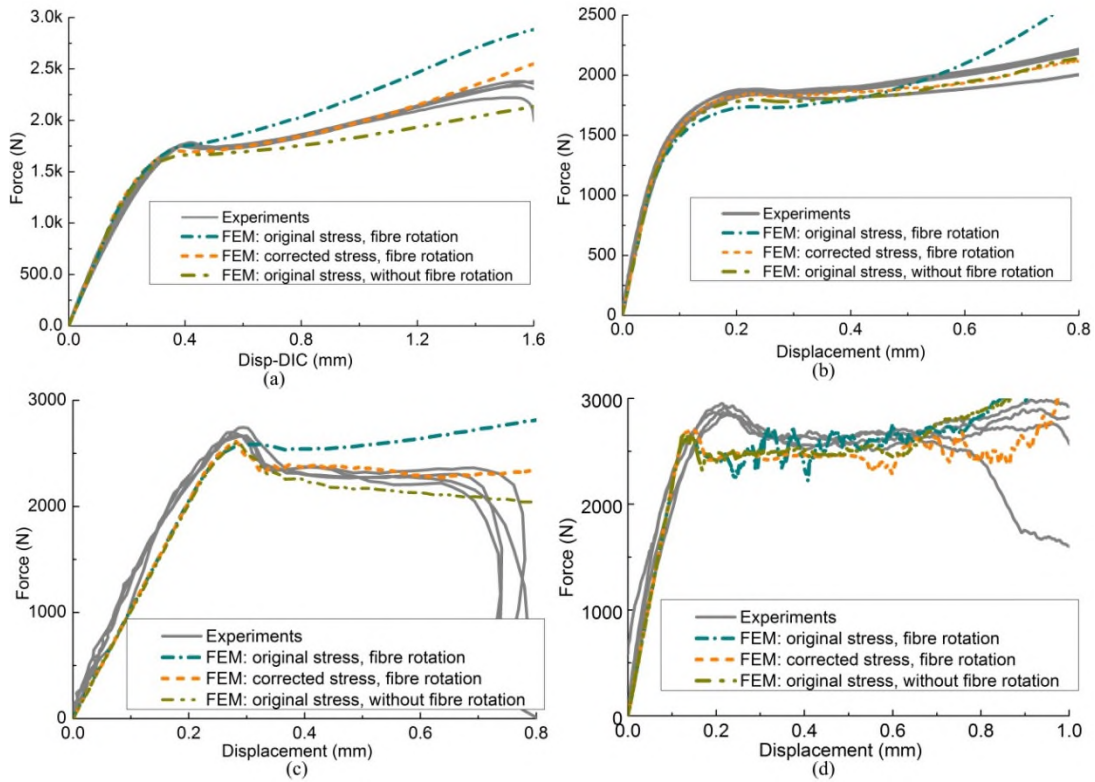


Fig.13 Comparison of force-displacement curves from experiments and simulations, (a) quasi-static tension; (b) quasi-static compression; (c) dynamic tension; (d) dynamic compression

All predicted force-displacement curves were compared with experiments in Fig.11. When the fibre orientation was updated during simulation, the original shear stress resulted in significant overestimation of the load in large strain stage. For tension tests, the load from simulations was higher than experimental value even at the small displacement stage. The fibre rotation has contributed to the originally determined shear properties, and the updating of material orientation may bring in additional fibre rotation, resulting in predicted load higher than the experimental value. Significant oscillations were observed in dynamic compression simulations with updating fibre orientation. Because the fibre rotation in compression decreased the element stiffness in global coordinates at the early stage of deformation. Besides, current commercial finite



element codes are not provided with enforcement mechanisms for the avoidance of unphysical deformation between neighbouring elements along fibre direction. Both factors tend to trigger concentration of plastic softening deformation, and caused premature dropping of the loading capacity.

The simulation without updating fibre orientation, using small-strain based shear stress, was also evaluated in this study. It provided good prediction in quasi-static compression tests. However, noticeable deviation from experimental results was shown in all tension simulations. This deviation may be induced by several factors not accounted for, such as the nonlinearity in transverse direction and rotation of fibre. Not taking into account the fibre orientation in constitutive models may compensate the fact that the contribution from fibre rotation has been included in the original shear response, making these simulations more accurate than above mentioned ones.

For the simulations with corrected shear properties and updated fibre orientation during computation, excellent correlations were achieved between simulations and experiments. This study did show that taking into account the fibre rotation is necessary to characterise experimentally more closely the true in-plane shear behaviour from uniaxial loading the  $\pm 45^\circ$  laminated samples, as well as that updating of fibre orientation during simulation would improve the accuracy of numerical models. Further improvement is achievable by relaxing the assumption adopted in this study that the transverse properties of the laminates remain undamaged.

When comparing the results against constitutive models readily available in commercial simulation packages, it is clear that not taking into account the rotation of fibre not only results in an increase in the apparent stress calculated using small strain theory, but it also causes the apparent reduction in stiffness in the original fibre orientation and a change in the in-plane distribution of stresses. With the growing demand for more accurate tools for predictive modelling of composite systems and

structures, the fibre rotation should be considered both in experiments and in numerical simulations, such that the true in-plane shear properties could be utilised. Further accounting for nonlinearities in the transverse direction, should lead to an even more accurate characterisation and modelling of the intrinsic material behaviour.

#### 4.5 Strain rate effect on failure mechanisms

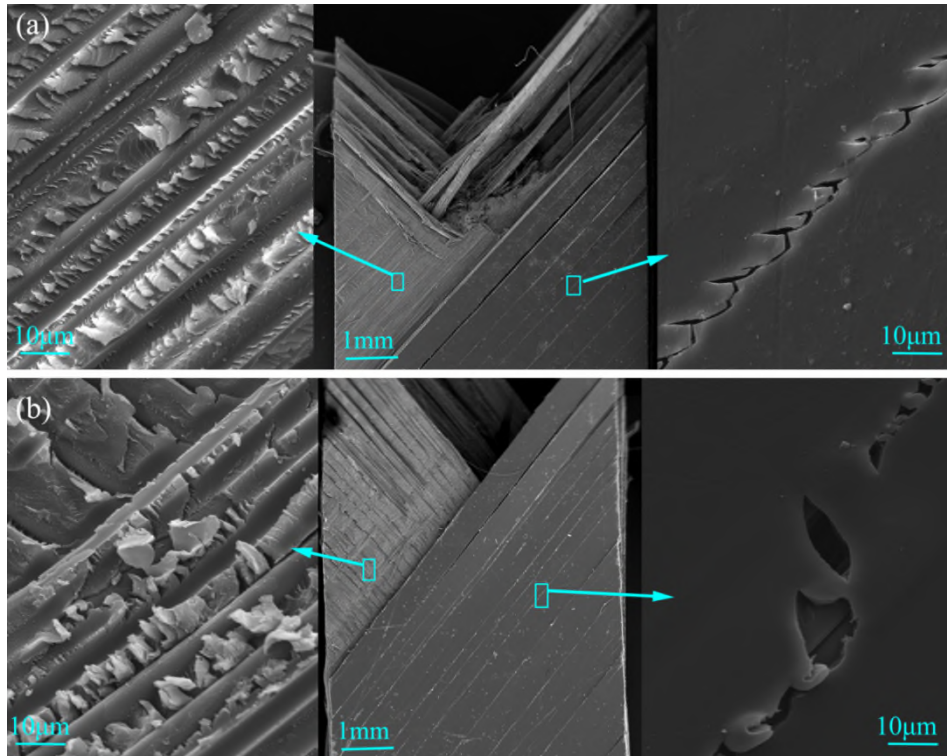


Fig.12 The deformation and fracture of tension samples from (a) dynamic tests and (b) quasi-static tests

The failure surface of tension samples were investigated as shown in Fig.12. In dynamic tests micro cracks at the surface ply took form of shear cusps with sharp edges, while shear cusps were not fully developed in quasi-static tests. Besides, the epoxy matrix was more severely distorted in lower loading rate, which indicates decreasing ductile failure behaviour with loading rate.

The delamination fractures initiated as cracks within the epoxy matrix in dynamic tests, and no significant fibre-matrix interface failure was observed. Shear cusps with

orientation perpendicular to the fibres were observed. Their size varied considerably, possibly controlled by the volume fraction of the matrix confined by fibres.

In quasi-static tests, shear cusps were mainly formed within matrix pockets of sufficient volume. Noticeable debonding between fibres and matrix was also identified. The strength of fibre-matrix interface may increase at higher loading rates above that of the epoxy matrix, which caused the migration of failure mechanisms from the interface into the matrix itself.

## **6. Conclusions**

The intrinsic, resin dominated nonlinear in-plane shear behaviour was characterised experimentally by  $\pm 45^\circ$  laminates loaded in tension and compression. The quantified shear response confirmed that the in-plane shear response can be captured with reasonably good accuracy using  $\pm 45^\circ$  laminates, for the shear strains below about 10%. It has been shown that fibre orientation should be taken into account at larger strains in order to quantify the true resin dominated nonlinear in-plane shear response.

The strain rate dependence has been investigated with tests at two distinct loading rates. The shear strength increased and failure strain decreased with strain rate, which should be attributed to a combination of viscous response of the polymeric resin and the change in failure mechanisms.

A constitutive model that incorporates reorientation of fibres as a function of shear deformation has been developed, thus enabling more accurate predictions of the rate dependent large deformation of long fibre reinforced composite laminates subjected to impact loading.

## **Acknowledgements**

The authors would like to acknowledge Rolls-Royce plc, for their continuing support through the Solid Mechanics University Technology Centre at the University of Oxford.

## References

- [1] Koerber H, Xavier J, Camanho PP. High strain rate characterisation of unidirectional carbon-epoxy IM7-8552 in transverse compression and in-plane shear using digital image correlation. *Mechanics of Materials*. 2010;42(11):1004-1019.
- [2] Daniel IM, Werner BT, Fenner JS. Strain-rate-dependent failure criteria for composites. *Composites Science and Technology*. 2011;71(3):357-364.
- [3] Fanteria D, Longo G, Panettieri E. A non-linear shear damage model to reproduce permanent indentation caused by impacts in composite laminates. *Composite Structures*. 2014;111:111-121.
- [4] Cousigné O, Moncayo D, Coutellier D, Camanho P, Naceur H. Numerical modeling of nonlinearity, plasticity and damage in CFRP-woven composites for crash simulations. *Composite Structures*. 2014;115:75-88.
- [5] Vogler M, Rolfes R, Camanho PP. Modeling the inelastic deformation and fracture of polymer composites – Part I: Plasticity model. *Mechanics of Materials*. 2013;59:50-64.
- [6] Pinho ST, Davila CG, Camanho PP, Iannucci L, Robinson P. Failure Models and Criteria for FRP Under In-Plane or Three-Dimensional Stress States Including Shear Non-Linearity. Hampton, Virginia: National Aeronautics and Space Administration; 2005. p. 69.
- [7] Mandel U, Taubert R, Hinterhölzl R. Mechanism based nonlinear constitutive model for composite laminates subjected to large deformations. *Composite Structures*. 2015;132:98-108.
- [8] Sket F, Enfedaque A, Alton C, González C, Molina-Aldareguia JM, Llorca J. Automatic quantification of matrix cracking and fiber rotation by X-ray computed tomography in shear-deformed carbon fiber-reinforced laminates. *Composites Science and Technology*. 2014;90:129-138.

- [9] Herakovich CT, Schroedter RD, Gasser A, Guitard L. Damage evolution in  $[\pm 45]_s$  laminates with fiber rotation. *Composites Science and Technology*. 2000;60:9.
- [10] Wisnom MR. The effect of fibre rotation in  $\pm 45^\circ$  tension tests on measured shear properties. *Composites*. 1995;26(1):8.
- [11] Gerlach R, Kettenbeil C, Petrinic N. A new split Hopkinson tensile bar design. *Int J Impact Eng*. 2012;50:63-67.
- [12] Miao Y-G, Li Y-L, Liu H-Y, Deng Q, Shen L, Mai Y-W, et al. Determination of dynamic elastic modulus of polymeric materials using vertical split Hopkinson pressure bar. *International Journal of Mechanical Sciences*. 2016;108-109:188-196.
- [13] Zhao H. Material behaviour characterisation using SHPB techniques, tests and simulations. *Comput Struct*. 2003;81(12):1301-1310.
- [14] Jumpasut A, Petrinic N, Elliott BCF, Siviour CR, Arthington MR. An Error Analysis into the Use of Regular Targets and Target Detection in Image Analysis for Impact Engineering. *Applied Mechanics and Materials*. 2008;13-14:203-210.
- [15] Marlett K. Hexcel 8552 IM7 Unidirectional Prepreg 190 gsm & 35%RC Qualification Material Property Data Report. Wichita: National institute for aviation research; 2011. p. 238.
- [16] Vanpaepegem W, Debaere I, Degrieck J. Modelling the nonlinear shear stress–strain response of glass fibre-reinforced composites. Part I: Experimental results. *Composites Science and Technology*. 2006;66(10):1455-1464.
- [17] de Morais AB, Cardoso CM, Pereira AB. Evaluation of in-plane ply shear properties from unidirectional plate torsion tests. *Composites Part A: Applied Science and Manufacturing*. 2013;53:168-175.
- [18] Mandel U, Taubert R, Hinterhölzl R. Three-dimensional nonlinear constitutive model for composites. *Composite Structures*. 2016;142:78-86.

[19] Goldberg RK, Roberts GD, Gilat A. Implementation of an associative flow rule including hydrostatic stress effects into the high strain rate deformation analysis of polymer matrix composites. Cleveland Ohio: Glenn Research Center, National Aeronautics and Space Administration; 2003.